Multimodal single cell analysis of the paediatric lower airway reveals novel immune cell phenotypes in early life health and disease

Jovana Maksimovic[1,2,9]*, Shivanthan Shanthikumar[2,3,4]*, George Howitt[1,9], Peter F Hickey[5,6], William Ho[5], Casey Anttila[5], Daniel V. Brown[5], Anne Senabouth[7,8], Dominik Kaczorowski[7,8], Daniela Amann-Zalcenstein[5], Joseph E. Powell[7,8], Sarath C. Ranganathan[2,3,4], Alicia Oshlack[1,9,10], Melanie R. Neeland[2,3,11#].

[1] Computational Biology Program, Peter MacCallum Cancer Centre, Parkville, VIC, Australia
[2] Respiratory Diseases, Murdoch Children's Research Institute, Parkville, VIC, Australia
[3] Department of Paediatrics, University of Melbourne, Parkville, VIC, Australia
[4] Respiratory and Sleep Medicine, Royal Children's Hospital, Parkville, VIC, Australia
[5] Cellular Genomics Projects Team, Advanced Technology and Biology Division, WEHI, Parkville, VIC, Australia
[6] Department of Medical Biology, University of Melbourne, Parkville, VIC, Australia
[7] Garvan-Weizmann Centre for Cellular Genomics, Garvan Institute of Medical Research, Sydney, NSW, Australia
[8] UNSW Cellular Genomics Futures Institute, University of New South Wales, Sydney, NSW, Australia
[9] Sir Peter MacCallum Department of Oncology, University of Melbourne, Parkville, VIC, Australia
[10] School of Bioscience, University of Melbourne, Parkville, VIC, Australia
[11] Molecular Immunity, Murdoch Children's Research Institute, Parkville, VIC, Australia
*Contributed equally
#Corresponding author

Corresponding author details:
Dr Melanie Neeland, PhD
Royal Children's Hospital, 50 Flemington Road, Parkville, VIC, Australia
Email: melanie.neeland@mcri.edu.au

Author contributions: JM, SS, SCR, AO and MRN designed the study. SS and SCR recruited the patients and collected samples. SS, CA, DVB, DK and MRN performed experiments and acquired the data. JM, SS, GH, PFH, WH, AS, AO and MRN analysed the data. JM, SS, DA-K, JEP, SCR, AO and MRN interpreted the data. All authors edited, revised, and approved the final manuscript.

Funding: The authors would like to acknowledge funding support from the Chan Zuckerberg Initiative (Inflammation Network), National Health and Medical Research Council of Australia Synergy Grant (1183640), and a Vertex Mentored Research Innovation Award. S.S is supported by a clinician-scientist fellowship from the Melbourne Children's Campus.

ABSTRACT

Respiratory disease is a major cause of morbidity and mortality in children worldwide. Many childhood respiratory diseases are characterised by chronic inflammation, however, the immune landscape of the paediatric airway remains uncharacterized. This is due to difficulties obtaining tissue-specific samples in early life as well as limited application of technologies that permit deep profiling from small sample volumes. Here, we employ multiomic single-cell sequencing to generate the first immune cell atlas of the paediatric lower airway with more than 44,900 cells across 12 preschool aged children. By integrating transcriptome-wide gene expression, assessment of 154 surface proteins, and functional pathway analysis, we extensively characterised 41 immune and epithelial cell populations present in the bronchoalveolar lavage of 11 children with cystic fibrosis and an age-matched healthy control. Paired spectral flow cytometry analysis of over 256,000 cells revealed high correlation in cell subset proportions and protein expression across the two techniques. We further revealed that paediatric alveolar macrophages consist of 13 functionally distinct sub populations, including previously undescribed populations enriched for IFN-α/β signalling, markers of vesicle production, and regulatory/repair function. Other novel immune cell populations not observed in previous studies of the adult lung include CD4 T cells expressing inflammatory signalling genes. Further, whilst we show no significant difference in overall cell proportions between CF and healthy lung, we observed significant differential gene expression in the alveolar macrophage population, including genes associated with lung inflammation (IL33, CCL15) and fibrosis (RBMS3, COL4A1, SPP1). Our work provides a comprehensive cellular analysis of the paediatric lower airway, reveals key immune signatures of early life lung disease, and provides a reference for investigations of respiratory immunity in children.

INTRODUCTION

Early childhood is a crucial period for the pulmonary system, characterised by rapid development and growth (1). The development of the pulmonary system in early childhood has lifelong implications and insults to this process can result in reduced pulmonary function in childhood, reduced peak pulmonary function in early adulthood, and a shorter descent to pulmonary insufficiency in later life. Childhood pulmonary diseases such as bronchopulmonary dysplasia (2), asthma and wheezing disorders (3), suppurative lung diseases (cystic fibrosis, idiopathic bronchiectasis, primary ciliary dyskinesia) (4) and interstitial lung diseases (5) are highly prevalent and all involve pulmonary inflammation. Current understanding of the mechanisms of pulmonary inflammation in early life in both health and disease is relatively limited, in part due to difficulty obtaining relevant biospecimens with enough volume to allow meaningful analysis.

Single-cell technologies offer the opportunity to better understand cell composition and function using small volume samples. Such technologies include single-cell RNA sequencing (scRNA-seq), multiomic single-cell sequencing (including cellular indexing of transcriptomes and epitopes by sequencing (CITE-seq)), and spectral flow cytometry (an advance on conventional flow cytometry as it allows analysis across the whole fluorescence spectrum). These technologies are increasingly used in pulmonary research (6, 7) but they have thus far primarily focused on analysis of lung tissue or epithelium, and samples collected in adult life. Consequently, pulmonary immune cells, which make up a small proportion of the tissue, as well as cell phenotypes in childhood, are currently underrepresented. Bronchoalveolar lavage (BAL), which is the most common method of sampling the lower airway in early life, is predominantly made up of immune cells and is the most relevant sample type for studies of pulmonary inflammation (8).

To improve our understanding of pulmonary immunity in early life, we aimed to apply novel multimodal single-cell analyses to BAL samples collected as part of clinical care in the first 6 years of life. We used samples collected from children with disease (cystic fibrosis) and one healthy control, and applied scRNA-seq, CITE-seq and spectral flow cytometry. The results offer several advancements in our understanding of immune cell composition of the childhood lung and how this differs to adult life, as well as highlighting key signatures of paediatric respiratory health and disease.

MATERIALS AND METHODS

Study participants

All subjects (n=11 with CF and n=1 healthy control) are enrolled in the AREST CF cohort at the Royal Children's Hospital, Melbourne, Australia (9). All families gave written and informed consent for their involvement in the AREST CF research program (HREC #25054), which includes collection of samples and clinical data. The healthy control participant had no history of lower airway disease and underwent bronchoscopy to investigate upper airway pathology. Supplementary Table 1 describes the demographics of study participants, and Figure 1A outlines the experimental design.

BAL sample collection and cryopreservation

All subjects underwent clinically indicated bronchoscopy. BAL was performed under general anaesthesia. Each BAL aliquot consisted of 1mL/kg (maximum 20mL) of normal saline being inserted via the working channel of the bronchoscope and then suctioned for return. BAL samples were placed on ice and processed immediately after the procedure. Samples were centrifuged at 300 x g for 10 min at 4°C. Cell-free BAL supernatant was then collected and stored at -80˚C for cytokine analysis. The cell pellet was resuspended in 10mL of media (RPMI supplemented with 2% fetal calf serum (FCS)), filtered through a 70uM filter and centrifuged at 300 x g for 7mins at 4°C. Supernatant was discarded and the cell pellet resuspended in media of for cell counting. The sample was then centrifuged at 300 x g for 10 min and resuspended in equal parts media and chilled freezing solution (FCS with15% dimethyl sulfoxide (DMSO)). The freezing solution was added to resuspended cells drop by drop on ice. The samples were transferred to cryovials, and then cooled at -1˚C per minute to -80 ˚C overnight before being transferred to liquid nitrogen for storage.

Single-cell sequencing and flow cytometry processing

1. <u>BAL cell thawing and live single cell sorting</u>

Cryopreserved BAL cells were thawed in 10mL media (RPMI supplemented with 10% heat-inactivated FCS) with 25U/mL benzonase at 37°C and centrifuged at 300xg for 10 min. The pellet was resuspended in 1mL PBS for cell counting. Following cell count, 9mL PBS was added to the tube and cells were centrifuged at 300 x g for 10 min. Supernatant was discarded

and the cell pellet resuspended in PBS for viability staining using live/dead fixable near infra-red viability dye (Invitrogen) according to manufacturers' instructions. The viability dye reaction was stopped by the addition of FACS buffer (2% heat-inactivated FCS in PBS 2mM EDTA) and cells were centrifuged at 400 x g for 5 min. Cells were resuspended in FACS buffer for live, single cell sorting using a BD FACSAria Fusion according to the gating strategy outlined in Supplementary Figure 1.

2. Sample and raw data processing for scRNA-seq (participants A1-D1)

Viable cells were sorted on a BD Influx cell sorter (Becton-Dickinson) into PBS + 0.1% bovine serum albumin and retained on ice. Sorted cells were counted and assessed for viability with Trypan Blue using a Countess automated counter (Invitrogen), and then resuspended at a concentration of 800-1000 cells/µL ($8x10^5$ to $1x10^6$ cells/mL). Final cell viability estimates ranged between 92-96%. Single cell suspensions were loaded onto 10X Genomics Single Cell 3' Chips along with the reverse transcription (RT) mastermix as per the manufacturer's protocol for the Chromium Single Cell 3' Library (10X Genomics; PN-120233), to generate single cell gel beads in emulsion (GEMs). Reverse transcription was performed using a C1000 Touch Thermal Cycler with a Deep Well Reaction Module (Bio-Rad) as follows: 55^{o}C for 2h; 85^{o}C for 5min; hold 4^{o}C. cDNA was recovered and purified with DynaBeads MyOne Silane Beads (Thermo Fisher Scientific; Cat# 37002D) and SPRIselect beads (Beckman Coulter; Cat# B23318). Purified cDNA was amplified as follows: 98^{o}C for 3min; 12x (98^{o}C for 15s, 67^{o}C for 20s, 72^{o}C for 60s); 72^{o}C for 60s; hold 4^{o}C. Amplified cDNA was purified using SPRIselect beads and sheared to approximately 200bp with a Covaris S2 instrument (Covaris) using the manufacturer's recommended parameters. Sequencing libraries were generated with unique sample indices (SI) for each chromium reaction. Libraries for all samples were multiplexed and sequenced across on 2×150 cycle flow cells on an Illumina NovaSeq 6000 (26bp (Read 1), 8bp (Index), and 98 bp (Read 2)).

The Cell Ranger Single Cell Software Suite (version 6.0.2) by 10x Genomics was used to process raw sequence data into FASTQ files. First, raw base calls from multiple flow cells were demultiplexed into separate pools of samples. Reads from each pool were then mapped to the GRCh38/hg38 genome (version 12) using STAR. The count data was processed and

analyzed in *R* as described below. This dataset will be henceforth referred to as the "scRNA-seq data.

3. Sample and raw data processing for CITE-seq (participants E2-L2)

Sorted live single cells were centrifuged at 400 x g for 5min at 4°C and resuspended in 25µL of cell staining buffer (BioLegend). Human TruStain FcX FC blocking reagent (BioLegend) was added according to manufacturers' instructions for 10min on ice. Each tube was made up to 100µL with cell staining buffer and TotalSeq Hashtag (HTO 1-8) reagents (BioLegend) were added to each sample for 20min on ice. Cells were washed with 3mL cell staining buffer and centrifuged at 400xg for 5min at 4°C. Supernatant was discarded and each sample resuspended at 62,500 cells/100µL following which 100µL of each sample were pooled into one tube. Pooled cells were centrifuged at 400xg for 5min at 4°C, supernatant discarded, and resuspended in 25µL cell staining buffer and 25ul of TotalSeqA Human Universal Cocktail v1.0 (BioLegend) for 30min on ice. This cocktail contains 154 immune related surface proteins. Cells were washed in 3mL cell staining buffer and centrifuged at 400xg for 5min at 4°C. Following two more washes, cells were resuspended in PBS + 0.04% BSA for Chromium captures.

Single-cell captures and library preparations were processed with the 10x Genomics Chromium single-cell Platform using the 10x Chromium Next GEM single-cell 3' Reagent V3.1 Dual Index kits (10x Genomics, USA) following the manufacturer's manual. In brief, pooled cells were counted and an estimated 40,000 cells were loaded per lane onto the 10x Chromium controller to form single-cell Gel Beads-in-Emulsion (GEMs) in duplicate. Captured cells were then lysed and barcoded and mRNA molecules were reverse transcribed to generate cDNA within the single GEMs. The barcoded cDNA was PCR-amplified and scRNA-seq libraries were constructed using the 10x 3'v3.1 library kits. The TotalSeq-A scADT-seq and scHTO-seq libraries were constructed as per manufacturer's instructions (BioLegend). The duplicate scRNA-seq, scADT-seq and scHTO-seq libraries were quantified by Tapestation 4200 D1000 chip (Agilent). Upon input normalisation, the 6 libraries were pooled and sequenced on the Illumina NextSeq500 sequencing platform to generate 400 million 2x75-bp paired-end reads.

Reads from each sample were processed using 10x Genomics Cell Ranger software (version 5.0.0). 'cellranger mkfastq' was used to demultiplex the Illumina sequencer's BCL files into FASTQ files. Next, 'cellranger count' was used to generate single-cell gene-count matrices against the 10x Genomics pre-built GRCh38 reference genome and transcriptome (2020-A (July 7, 2020) version). All subsequent analysis was performed in R (version 4.0.3) (R Core Team. R. A language and environment for statistical computing, 2020) with Bioconductor (version 3.12) (10). The DropletUtils package (version 1.10.3) (11) was used to create a SingleCellExperiment object from the Cell Ranger output directories and to identify non-empty droplets. Samples were demultiplexed based on the hashtag oligo (HTO) counts using the 'hashedDrops' function from DropletUtils with the default parameters. This was performed separately for each capture. In parallel, samples were demultiplexed using their genetic data by running cellsnp-lite (v1.2.0) (12) and Vireo (v0.5.6) (13). Specifically, reads from non-empty droplets were genotyped at 36.6M SNPs with minor allele frequency (MAF) > 0.0005 in the 1000 Genomes Project (http://ufpr.dl.sourceforge.net/project/cellsnp/SNPlist/genome1K.phase3.SNP_AF5e4.chr1toX.hg38.vcf.gz) using cellsnp-lite and then vireo assigned each cell barcode to 1 of 8 donors, doublets, or unassigned based on these genotypes. This was performed separately for each capture and then pairs of donors were matched across captures by identifying the best match between captures based on the genotype profile of each donor. As more cells were confidently assigned to donors using genetic demultiplexing, the genetic assignments were used for downstream analysis. Almost all genetic assignments corresponded to a single HTO, which was then used to link each cell's genetic assignment to a study participant (Supplementary Table 2). This dataset will be henceforth referred to as the "CITE-seq data".

4. Flow cytometry protocol and analysis (participants F2-L2)

BAL samples from seven participants had remaining cells for flow cytometry analysis. Following viability stain as described above, cells were then resuspended in human FC-block according to manufacturers' instructions for 5 minutes at room temperature. The antibody cocktail (Supplementary Table 3) made up at 2X concentration was added 1:1 with the cells and incubated for 30 minutes on ice. Following staining, cells were washed with 2 mL FACS buffer and centrifuged at 400 x g for 5min. Cells were then resuspended in 2% PFA for a 20min fixation on ice, washed, and resuspended in 150µl FACS buffer for acquisition using a 5L Cytek Aurora. Our protocols for the collection and processing of paediatric BAL for

single-cell analysis are publicly available at https://www.protocols.io/workspaces/earlyAIR. Flow cytometry results were analysed (manual gating, UMAP) using FlowJo Version 10.8.1 software. Manual gating was performed according to the gating strategy depicted in Supplementary Figure 1. UMAP analysis was conducted using a concatenated file containing all live single cells (total 256, 278) from each individual using default parameters within FlowJo. Mean expression levels of each protein were exported from FlowJo for each manually gated cell type, following which heatmap plotting and unsupervised hierarchical clustering was performed using the Morpheus heatmap tool (https://software.broadinstitute.org/Morpheus).

Single-cell sequencing data analysis

The "scRNA-seq data" was generated from 4 individuals' samples (participants A1-D1), across 4 captures (1 control sample, 3 CF samples). The "CITE-seq data" was generated from a further 8 individuals' samples (participants E2-L2) multiplexed across 2 captures (8 CF samples). Both datasets were similarly processed using the R statistical programming language (version 4.1.0). As previously described for the "CITE-seq data" in Methods Section 2 of *Single-cell sequencing and flow cytometry processing*, the DropletUtils package (version 1.14.1) (10) was used to identify non-empty droplets in the "scRNA-seq data". This was performed separately for each capture. There were 33,538 non-empty droplets across the 4 samples for the "scRNA-seq data" and 36,601 across the 8 samples for the "CITE-seq data". Quality control was performed on each sample independently by examining the total cell number, the total unique molecular identifier (UMI) count distributions, the number of unique genes detected, and the proportions of ribosomal and mitochondrial gene counts per cell. Droplets with unusually large mitochondrial proportions were identified and removed from each sample. Outliers were detected based on being more than 3 median absolute deviations (MADs) from the median value of the metric across all droplets in each sample. DropletQC (14) was used to detect and tag additional empty droplets; there was convincing evidence of additional empty droplets present in the "scRNA-seq data". The filtered droplets from the "scRNA-seq data" and "CITE-seq data" were then combined across 32,732 unique genes, resulting in a total of 54,106 unique droplets. 1,558 "uninformative" genes, such as mitochondrial genes, ribosomal genes, sex chromosome genes and pseudogenes, were then removed. Droplets that were unassigned or doublets based on their genetic profile were discarded, along with HTO doublets and the additional DropletQC empty droplets originating

from the "scRNA-seq data", leaving 45,590 droplets. 19,120 genes were retained for downstream analysis after genes expressed in less than 20 cells were discarded.

The droplets were then automatically annotated with cell type labels from the Human Lung Cell Atlas (HLCA) versions 1 (https://app.azimuth.hubmapconsortium.org/app/human-lung) and 2 (https://app.azimuth.hubmapconsortium.org/app/human-lung-v2) using versions 0.4.1 and 0.4.4 of the Azimuth online application, respectively. The annotated cells were then split into 3 separate data subsets based on their HLCA level 3 labels: "macrophage" (33,161 cells), "T/NK" (6,462 cells) and all "other" cells (5,922 cells), to facilitate confirmation of cell identity and identification of cellular subpopulations. Genes without associated Entrez identifiers were removed at this stage, leaving 16,001 genes for subsequent analyses.

Each data subset ("macrophage", "T/NK" and "other" cells) was independently normalised with SCTransform (15), integrated, scaled, and clustered using Seurat (version 4.0.6) (16-19). Data integration of the 12 samples for each subset of cells was performed using reciprocal principal components analysis (RPCA) with the 4 "scRNA-seq data" samples set as references, 30 dimensions, 3000 features and 20 neighbours for anchor picking. For the "other" cells subset, the number of neighbours to consider when weighting anchors (k.weight) was set to the smallest number of cells in a single sample minus one. The cells in each subset were clustered using the smart local moving (SLM) algorithm with 30 principal components. Ten resolutions between 0.1 and 1 were explored using the clustree (20) package (version 0.4.4); a resolution of 1 was selected for downstream analysis of each data subset. This strategy resulted in 23, 18, and 23 subclusters in the "macrophage", "T/NK" cell, and "other" cell data subsets, respectively. The clusters were visualised using Uniform Manifold Approximation and Projection (UMAP). The quality of each cluster was assessed by examining their Azimuth prediction score distributions, total UMI count distributions and the distributions of the total number of unique genes detected.

Marker gene analysis was performed for each cluster, in each of the data subsets, as previously described in Sim et al. 2021 (21), except that a 1.5-fold change cutoff was used for the TREAT test. Gene set enrichment analysis of the REACTOME gene sets (https://www.gsea-msigdb.org/gsea/msigdb/collections.jsp) was performed for each cluster in each data subset using 'camera' (22). The antibody derived tag (ADT) data associated with the "CITE-seq data" was normalised using the 'dsb' (23) method (version 1.0.1) following their suggested workflow (https://cran.r-

project.org/web/packages/dsb/vignettes/end_to_end_workflow.html). The combination of the top marker genes, REACTOME pathways and ADT expression for each cluster was used to assign them cellular and/or functional identities. The clusters were then consolidated using these manually assigned labels. Cells in clusters with no obvious cellular and/or functional identity and poor quality control metrics were removed from subsequent analyses. This strategy resulted in 14, 12 and 15 manually annotated clusters in the "macrophage", "T/NK" and "other" subsets, respectively. Broad cell type labels were also manually assigned to each cluster, resulting in a total of 13 broad cell type labels across the three data subsets. Marker genes for the consolidated subpopulations in each data subset were identified using the 'Cepo' (24) method. Differences in composition of macrophage subpopulations between the control and CF samples were assessed for statistical significance using the 'propeller' test (25) from the speckle (version 0.0.3) package (https://github.com/Oshlack/speckle).

The "macrophage", "T/NK" and "other" cell data subsets were subsequently combined resulting in a total of 44,972 cells. The data were then normalised, integrated, scaled and clustered as previously described herein. The subpopulation and broad cell type labels were visualised using UMAP. Marker genes for the broad cell types were identified using the 'Cepo' method. Differences in composition of broad cell types between the control and CF samples were assessed for statistical significance using 'propeller' (25). Cell type proportions estimated by flow cytometry and scRNA-seq were compared using the 'propeller' approach; the proportions were arcsin transformed and linear models fitted using limma, taking the paired individual samples into account. The Benjamini-Hochberg procedure (26) was used to adjust for multiple testing.

Pseudobulk samples (27) were generated by adding the counts for each sample, for each cell type. Genes with very low counts were filtered out using the 'filterByExpr' function from the edgeR package (28) based on the strategy described in Chen et al. (2016) (29), leaving 11,429 genes. Differential gene expression analysis within macrophages, between the control and CF samples, was performed using limma (30) as described in Sim et al. 2021 (21). Briefly, the data were transformed using voom (31) with cyclic-loess normalisation; significantly differentially expressed genes were then identified using moderated *t* tests, incorporating robust (32) empirical Bayes shrinkage of the variances, followed by TREAT tests (33) with a log-fold change cutoff of 0.5 at a false discovery rate (FDR) less than 0.05. Enrichment of

gene ontology (GO) terms and REACTOME pathways was tested using 'gsaseq' from the missMethyl package (34) (version 1.28.0), taking gene length into account.

All of the code, figures and outputs for the analyses described herein can be viewed at the following workflowr (35) (version 1.7.0) analysis website on GitHub: https://oshlacklab.com/paed-cf-cite-seq/. The code, as well as all necessary inputs and outputs can be cloned from the GitHub repository associated with the analysis website: https://github.com/Oshlack/paed-cf-cite-seq.

RESULTS AND DISCUSSION

1. Broad immune and epithelial cell profile of the paediatric lung

Unsupervised clustering of single-cell sequencing data and cell annotation using marker gene analysis revealed the following transcriptionally distinct broad cell populations in paediatric BAL: alveolar macrophages, proliferating macrophages, monocytes, dendritic cells, neutrophils, B cells, CD4 T cells, CD8 T cells, NK cells, NK-T cells, proliferating NK/T cells, innate lymphocytes, γδ T cells, mast cells, epithelial cells and endothelial cells (Figure 1B). Macrophages were the most abundant cell type identified, followed by CD4 T cells, proliferating macrophages, CD8 T cells, dendritic cells, innate lymphocytes, B cells, monocytes, NK cells and neutrophils. Epithelial cells, NK-T cells, γδ T cells, proliferating NK/T cells, mast cells, and endothelial cells were rarer, and not detected in all individuals (11/12, 11/12, 9/12, 10/12, 6/12, and 2/12 respectively) (Figure 1C).

The five most significant marker genes for each broad cell population are shown in Figure 1D. These marker genes included those described previously for respective cell populations; macrophages (CYP27A1, MS4A4A and PPARG), proliferating macrophages and proliferating NK/T cells expressing cyclic genes (PCLAF and MKI67), B cells (CD19, MS4A1), CD4 T cells (CD3D, CD3E), CD8 T cells (CD8A, CD8B), innate lymphocytes (LEF1, XCL1), γδ T cells (TRGC1, GZMK), NK cells (KLRC1, XCL1), NK-T cells (KLRC1, CD3D), dendritic cells (CLEC10A, CD1E), monocytes (CSF1R, FCGR2B), mast cells (TPSAB1, CPA3), epithelial cells (AGR2, KRT17), and endothelial cells (SPARCL1, ACKR1) (6, 7, 36-38).

Annotation of each cell population was further confirmed by analysis of expression of TotalSeq ADTs (Figure 1E). Alveolar macrophages expressed myeloid lineage proteins CD172α, CD11c, CD71, HLA-DR, and CD169 as previously reported for alveolar macrophages in adults (39, 40). Monocytes were distinguished from macrophages based on the pan monocyte marker CD14, as well as the lack of CD71 and CD169. Dendritic cells expressed CD11c, CD172α and CD1c; and mast cells expressed known protein markers FcεR1α, CD63, and IgE (41). Cells annotated as lymphoid lineage by marker genes expressed expected lineage proteins, including B cells ($CD19^+CD20^+$), CD4 T cells ($CD3^+CD5^+CD4^+$), CD8 T cells ($CD3^+CD5^+CD8^+$), γδ T cells ($CD3^+TCRV\delta2^+$), NK cells ($CD3^-CD56^+$) and NK-T cells ($CD3^+CD56^+$). Epithelial cells were positive for tissue resident marker CD49b.

2. Comparison of cell proportions by single-cell sequencing and flow cytometry

To investigate how results obtained by single-cell sequencing compared to those obtained by flow cytometry, we directly compared the 7 BAL samples analysed with both techniques. Our flow cytometry panel permitted identification of alveolar macrophages, monocytes, dendritic cells, neutrophils, B cells, CD4 T cells, CD8 T cells and airway epithelial cells across 256,000 live, single cells (Figure 2A). Proportions of alveolar macrophages, monocytes, B cells, CD4 T cells, CD8 T cells and airway epithelial cells were generally consistent between the two techniques for each individual (Figure 2B-C). However, we observed statistically significant differences in the proportion of neutrophils (fold change flow vs scRNA-seq: 1.2, FDR=0.006) and dendritic cells (fold change flow vs scRNA-seq: -1.17, FDR=0.019) (Figure 2C). Due to the low RNA content of neutrophils and previously reported challenges in characterising these cells using single-cell technologies such as 10x (42), the higher proportion of neutrophils detected by flow cytometry was unsurprising. The reduced proportion of dendritic cells detected by flow cytometry compared to scRNA-seq was likely due to the absence of key dendritic cell subset markers CD1c and CD123 in our flow cytometry panel. Comparable protein expression patterns were observed for common surface markers CD3, CD8, CD4, CD19, CD16, CD45, HLADR, CD11c, CD14, CD47 and CD279 across the two techniques (Figure 2D). Of note, our flow cytometry panel also included several surface proteins not available in the TotalSeq-A cocktail, including CD206 for alveolar macrophages, CD15 and CD66b for neutrophil subtyping, and EPCAM for airway epithelial cells (Figure 2C). Airway macrophages showed auto-fluorescent signatures in flow cytometry data as we and others have described previously (8, 43).

Despite the aforementioned challenges of studying neutrophils by scRNA-seq, we identified a population of 252 neutrophil-like cells, to which 7 donors contributed more than 10 cells and the remaining 5 fewer than 10 cells. This population mapped to neutrophils identified by a publicly available and annotated scRNA-seq dataset of the adult lung (44) and expressed inflammatory genes including those encoding for S100 proteins and the IL-1 signalling pathway. Protein expression on these cells included CD35, CD55, CLEC12A, CD48, and a lack of HLA-DR (Figure 1E). CD55 and CD35 are known to be involved in neutrophil phagocytosis (45). Cells in this neutrophil-like population also shared gene and protein features with monocytes (genes: FCN1, CD300E; proteins: CD11b and CD14), which has

been described for neutrophils previously (46-49). A more extensive panel of neutrophil-specific ADTs that are not currently included in the TotalSeq A cocktail could be used to further characterise this cell type; for example, CD15 and CD66b are protein markers that we use to distinguish BAL neutrophils from monocytes by flow cytometry (43). We show by flow cytometry that BAL neutrophils can be further subtyped based on CD16 and CD66b expression, with $CD16^{-}CD66b^{high}$, $CD16^{+}CD66b^{high}$ and $CD16^{+}CD66b^{low}$ subsets identified (Supplementary Figure 1, Figure 2D).

An inherent limitation of our data is that our samples were cryopreserved and thawed prior to analysis. This process is known to deplete granulocytes; however, we have shown in previous work that cryopreservation of BAL should not affect the yield of other immune cell populations (8). As is the case with most clinical studies, our sampling times are unpredictable in nature and cryopreservation is unavoidable.

3. Identification of functionally distinct alveolar macrophage subpopulations

As alveolar macrophages are the most abundant immune cell in BAL and are known to undergo significant functional development in early life (50), we performed a subclustering analysis of our broad alveolar macrophage population (Figure 3A-B). Subclusters were annotated based on marker gene analysis (Figure 3C), ADT protein expression (Figure 3D), and with reference to what has been described in previous scRNA-seq literature. To further confirm annotations and understand subpopulation functionality based on DEGs, we also performed REACTOME pathway enrichment analyses for each subtype (51). A list of enriched REACTOME pathways in each population is provided in Supplementary Table 4, and a full list of cluster marker genes can be found in extended data file 1.

Our analysis revealed 13 functionally distinct subpopulations of alveolar macrophages, of which several have recently been described in adults. Subtypes characterised in the adult lung and also identified here include intermediate macrophages expressing both monocyte and macrophage genes (macro-int) (7), chemokine-expressing macrophages (macro-CCL) (7), interstitial macrophages, and metallothionein-expressing macrophages (macro-MT) (7) (Figure 3B). The macro-CCL population in our dataset was enriched for the chemokine-receptor-bind-chemokines REACTOME pathway, and expressed genes for chemokines CCL4, CCL20, CCL23, CXCL5, CXCL8, CXCL9 and CXCL10, further confirming its annotation. Interestingly, macro-interstitial, macro-CCL, and macro-int cells expressed high

protein levels of CD54 (ICAM1), a transmembrane glycoprotein receptor known to play an important role in migration of leukocytes to sites of inflammation (52) (Figure 3D). In addition to expressing genes associated with both monocytes and macrophages, the macro-int population also expressed proteins associated with both populations, including CD11b, CD48 and intermediate levels of CD14 (Figure 3D).

The most abundant functional macrophage subcluster in our data, at a median of 12.8% of macrophages, was a population expressing IFN-α/β signalling genes that we denoted as macro-IFN-α/β. This cluster was characterised by expression of IFI27 and IGF1 and enriched for REACTOME pathways including interferon-alpha-beta signalling. The next most abundant subcluster we defined as macro-lipid (9.32% of macrophage), based on enrichment of genes (NUPR1, RBP4) and REACTOME pathways associated with lipid digestion and transport. The macro-int population described above made up 8.65% of macrophages. We also identified other novel rare macrophage subpopulations expressing markers of: viral-response (IFI44L, IFIT1, RSAD2, CXCL10) denoted as macro-viral; vesicle production (AZU1, PLAC8) denoted as macro-vesicle; cholesterol biosynthesis related genes (MSM01, FDFT1) denoted as macro-cholesterol; regulatory function (ATF4, GDF15) denoted as macro-reg; response to DNA damage (CDKN1A, MDM2) denoted macro-repair; and T cell interaction (IL32, TRAC, CD2) denoted as macro-T (Figure 3C). The macro-T population expressed macrophage markers CD169, CD172α and CD71 whilst also expressing proteins CD8, CD2, and CD103 (Figure 3D). Whilst unconventional, a growing body of evidence regarding novel macrophage subpopulations expressing T cell markers has recently emerged (53, 54). All macrophage subpopulations were identified in each individual (Figure 3B), and there was no statistically significant difference in subcluster proportions between healthy and CF samples.

Overall, our data suggest macrophages in the early lung are highly activated. This is evidenced by the identified subclusters, but also enrichment for a range of inflammatory pathways including IL-1 signalling, IFNa/b activation, chemokine signalling, and antiviral responses. This is consistent with prior studies showing that the upper airway of children demonstrates a baseline pre-activated state, characterised by upregulation of antiviral and inflammatory signatures compared to adults (55). Our findings demonstrate that children may have these pre-activated signatures in the lower airway as well. This may have important implications for pathogen response given that the increase in upper airway interferon

signatures is thought to contribute to the milder illness with SARS-COV-2 infection seen in children. Whilst these inflammatory signatures were observed in our healthy and CF samples, further work characterising the baseline activation state from samples of healthy children are required.

4. Inflammatory CD4 T cell subsets in the paediatric lower airway

Our initial gene and protein expression analysis in Figure 1 showed broad populations of CD4 T cells, CD8 T cells, innate lymphocytes, NK cells, NK-T cells and γδ T cells in BAL of children. As with macrophages, we next explored heterogeneity within these T/NK subsets using a subclustering approach (Figure 4). Our analysis revealed both known and novel subtypes, using marker gene (Figure 4B, extended data file 2), ADT protein expression (Figure 4C) and REACTOME pathway analysis (Supplementary Table 5). Previously reported subtypes observed by single-cell RNA sequencing of adult lung samples that we also observed in our analysis were CD8 Trm, CD8-GZMK, CD4 Treg, γδ T cells, NK cells, NK-T cells, innate lymphocytes and proliferating NK/T cells (6, 7, 44).

Two subtypes of CD8 T cells (CD8 Trm and CD8-GZMK) and NK-T cells showed gene and protein markers of lung tissue residency, including surface expression of CD103 and CD49a (56) (Figure 4B-C). Conversely, CD4 T cell subsets, NK cells, innate lymphocytes, and γδ T cells were negative or only weakly positive for CD103 and CD49a, suggesting they were recently recruited from the circulation. Both CD8 Trm and CD8-GZMK subtypes expressed genes encoding for cytotoxic proteases GZMA, GZMB, GZMH, GZMM however CD8-GZMK was the only CD8 subtype to express GZMK. Recent work has shown that patterns of cytotoxic molecule expression relate to CD8 T cell differentiation stage, with a lack of GZM expression observed in naïve CD8 T cells, the majority of memory CD8 T cells co-expressing GZMA/B/M, and a low number of intermediately-differentiated CD8 T cells expressing CZMK (57). CD4 T follicular helper (CD4-TFH) cells expressing TFH genes SCGB3A1 and PD1 signalling (58) were also identified, however only in one individual (Supplementary Figure 2A).

To our knowledge, we are the first to describe subtypes of CD4 T cells enriched for IFN and NFκB signalling genes in the lung. Features of the CD4 T-IFN subtype include marker genes IFIT1, IFIT3, RSAD2 (Figure 4B) as well as REACTOME enrichment for interferon and antiviral pathways. Features of the CD4 T-NFκB subtype include marker genes TNFRSF4,

TNFRSF18, NFKB2 (Figure 4B) as well as REACTOME enrichment for several NFκB activation and signalling pathways (Supplementary Table 5). These inflammatory CD4 T cells were observed in samples from both health and disease (cystic fibrosis) (Supplementary Figure 2A). This highlights that these cells may represent a unique characteristic of the paediatric lung and adds further evidence to the concept that the paediatric lower airway is primed for inflammatory responses.

5. Defining rare cells

A final subclustering analysis of all other cells (not macrophages, not T/NK) revealed further heterogeneity within the rarer DC, B cell and epithelial cell clusters (Figure 5, Supplementary Table 6, Supplementary Figure 2B, extended data file 3). DCs were separated into conventional DC (cDC1 and cDC2), plasmacytoid DC, and migratory DC, based on previously described marker genes (6) and protein expression. cDC1 expressed CLEC9A gene and CD141 protein, whilst cDC2 expressed CD1c (59-61). Plasmacytoid DC expressed plasmacytoid surface marker CD123, were negative for conventional markers CD1c and CD141, and marker genes included CLEC4C and GZMB. Plasma B cells were also identified, characterised by key marker genes (JCHAIN, MZB1, TNFRSF17) as well as protein expression of plasma markers CD27 and CD38 (62) (Figure 5B-C).

Whilst BAL predominantly samples immune cells of the lower airway, a small fraction of airway epithelial cells was also captured. We identified 4 subtypes of airway epithelial cells: ciliated epithelial cells, basal epithelial cells and 2 clusters containing cells of a goblet/club phenotype. These were annotated using the recently released Human Lung Cell Atlas (HCLA) (6). The ciliated epithelial cell cluster expressed marker genes which are exclusively expressed by ciliated columnar cells of the tracheobronchial tree, and multiciliated epithelial cells in the HLCA. The basal epithelial cells expressed well-validated marker genes KRT17, KRT5, and KRT6a. Two distinct populations expressing a mixture of goblet and club cell marker genes were identified. One cluster, denoted as goblet/club cells, expressed marker genes including MUC5AC, TFF1, AZGP1, FST, and SYT8 which are expressed by club, goblet and mucus secreting cells. Another cluster, denoted as tracheobronchial goblet/club cells, expressed the marker gene TSPAN8 which is a HCLA marker gene for both club and goblet cells from the lower airway.

6. Altered macrophage gene expression in cystic fibrosis

Previous work in adults showed altered single-cell gene expression signatures in BAL macrophages from patients with chronic obstructive pulmonary disease compared to healthy controls (63). Furthermore, macrophages have been shown to play a role in adult CF lung disease, demonstrating both hyper-inflammatory properties and impaired phagocytic capacity (64, 65). As such, we next explored differential gene expression in alveolar macrophages from CF samples compared to an age matched healthy control (Figure 6). We recognise the limitations of a single control sample and highlight that further studies in larger patient cohorts are required. In our exploratory analysis we showed that alveolar macrophages from children with CF show higher expression of genes associated with lung inflammation (IL33, CCL15, CCL7. S100A12) (66-69), lung disease and fibrosis (RBMS3, PRRX2, SPP1, FBN1) (66, 70-72), and extracellular matrix formation (COL4A1 and its receptor ITGB1) (63, 73). Furthermore, compared to control macrophages, CF macrophages show reduced expression of genes associated with phagocytosis including IGHA2, IGHG4, IGHM (74), indicating impaired function (Figure 6A). Within the samples from children with CF, we observed significant patient-to-patient variability in gene expression which is not explained by sex or age (Figure 6B). This variability may be associated with factors such as disease-causing genotype, modifier genes, treatments received, and comorbidities (i.e. chronic infections), further highlighting the need for assessment of samples from larger cohorts. Recent work in adults with CF used scRNA-seq to show that CF sputum samples were characterised by a relative abundance of monocyte-derived macrophages and activated monocytes when compared with healthy controls (75) . The authors also showed that CF sputum granulocytes exhibited an immature hyperinflammatory phenotype with reduced expression marker genes of phagocytosis. Combined, these exploratory data provide novel insights into disease pathophysiology and highlight the utility of next generation single-cell technologies in defining mechanisms of pulmonary disease.

CONCLUSIONS

This is the first single-cell analysis of bronchoalveolar lavage from early life and includes both RNA and protein. These novel data fill a substantial gap in existing pulmonary scRNA-seq data. Early life is a crucial period of development for both epithelial and immune cells of the pulmonary system. For example, unlike other organs such as the skin, liver and brain where the transcriptome of resident macrophages from fetal and adult life are very similar, there are substantial differences in the gene expression profiles of fetal and adult lung

resident macrophages (76). This highlights childhood as a period where fetal lung resident macrophages must develop before eventually exhibiting an adult phenotype.

The recent release of the HLCA contained a core dataset derived from samples of 107 individuals, however the youngest of these individuals was 10 years old (6). The HLCA also included an extended dataset, however only 6 of the 338 (1.7%) were from individuals 6 years or less and these samples were not analysed separately to identify specific developmental changes. Previous scRNA-seq datasets involving people with CF have also focused only on adult samples. Furthermore, the majority of published pulmonary scRNA-seq datasets are derived from lung tissue or epithelium, allowing unparalleled analysis of these cell types but limiting the assessment of the pulmonary immune system. The use of bronchoalveolar lavage in our study allowed robust profiling of lower airway immune cell populations.

By integrating transcriptome-wide data, assessment of highly multiplexed surface proteins, and functional pathway analysis, we extensively characterised 41 cell populations in the bronchoalveolar lavage of children aged 3-6 years. We revealed several novel cell subtypes, most notably functional macrophage subpopulations and inflammatory CD4 T cells. Our analysis of paired cell surface protein expression using TotalSeq ADTs and spectral flow cytometry further extends current knowledge of lung cell types and provides within-study validation of our transcriptomic findings. In addition, our initial analysis identified signatures of early life cystic fibrosis lung disease but was limited by the inclusion of only one healthy control due to the difficulty in obtaining lower airway samples from healthy children. Further work investigating these signatures in larger patient cohorts is required and will be facilitated by programs such as the Pediatric Networks for the Human Cell Atlas.

This study provides the first transcriptional profile of early life lower pulmonary samples and provides a reference dataset for researchers investigating the pulmonary immune system in childhood and its role in health and disease.

REFERENCES

1. Stocks J, Hislop A, Sonnappa S. Early lung development: lifelong effect on respiratory health and disease. *Lancet Respir Med* 2013; 1: 728-742.
2. Holzfurtner L, Shahzad T, Dong Y, Rekers L, Selting A, Staude B, Lauer T, Schmidt A, Rivetti S, Zimmer KP, Behnke J, Bellusci S, Ehrhardt H. When inflammation meets lung development-an update on the pathogenesis of bronchopulmonary dysplasia. *Molecular and cellular pediatrics* 2022; 9: 7.
3. Bush A. Pathophysiological Mechanisms of Asthma. *Front Pediatr* 2019; 7: 68.
4. Chang AB, Boyd J, Bell L, Goyal V, Masters IB, Powell Z, Wilson C, Zacharasiewicz A, Alexopoulou E, Bush A, Chalmers JD, Fortescue R, Hill AT, Karadag B, Midulla F, McCallum GB, Snijders D, Song WJ, Tonia T, Grimwood K, Kantar A. Clinical and research priorities for children and young people with bronchiectasis: an international roadmap. *ERJ Open Res* 2021; 7.
5. Rosewich M, Zissler UM, Kheiri T, Voss S, Eickmeier O, Schulze J, Herrmann E, Dücker RP, Schubert R, Zielen S. Airway inflammation in children and adolescents with bronchiolitis obliterans. *Cytokine* 2015; 73: 156-162.
6. Sikkema L, Strobl D, Zappia L, Madissoon E, Markov N, Zaragosi L, Ansari M, Arguel M, Apperloo L, Bécavin C, Berg M, Chichelnitskiy E, Chung M, Collin A, Gay A, Hooshiar Kashani B, Jain M, Kapellos T, Kole T, Mayr C, von Papen M, Peter L, Ramírez-Suástegui C, Schniering J, Taylor C, Walzthoeni T, Xu C, Bui L, de Donno C, Dony L, Guo M, Gutierrez A, Heumos L, Huang N, Ibarra I, Jackson N, Kadur Lakshminarasimha Murthy P, Lotfollahi M, Tabib T, Talavera-Lopez C, Travaglini K, Wilbrey-Clark A, Worlock K, Yoshida M, Consortium LBN, Desai T, Eickelberg O, Falk C, Kaminski N, Krasnow M, Lafyatis R, Nikolíc M, Powell J, Rajagopal J, Rozenblatt-Rosen O, Seibold M, Sheppard D, Shepherd D, Teichmann S, Tsankov A, Whitsett J, Xu Y, Banovich N, Barbry P, Duong T, Meyer K, Kropski J, Pe'er D, Schiller H, Tata P, Schultze J, Misharin A, Nawijn M, Luecken M, Theis F. An integrated cell atlas of the human lung in health and disease. *bioRxiv* 2022: 2022.2003.2010.483747.
7. Madissoon E, Oliver AJ, Kleshchevnikov V, Wilbrey-Clark A, Polanski K, Orsi AR, Mamanova L, Bolt L, Richoz N, Elmentaite R, Pett JP, Huang N, He P, Dabrowska M, Pritchard S, Tuck L, Prigmore E, Knights A, Oszlanczi A, Hunter A, Vieira SF, Patel M, Georgakopoulos N, Mahbubani K, Saeb-Parsy K, Clatworthy M, Bayraktar OA, Stegle O, Kumasaka N, Teichmann SA, Meyer KB. A spatial multi-omics atlas of the human lung reveals a novel immune cell survival niche. *bioRxiv* 2021: 2021.2011.2026.470108.
8. Shanthikumar S, Burton M, Saffery R, Ranganathan SC, Neeland MR. Single Cell Flow Cytometry Profiling of Bronchoalveolar Lavage in Children. *American journal of respiratory cell and molecular biology* 2020.
9. Sly PD, Gangell CL, Chen L, Ware RS, Ranganathan S, Mott LS, Murray CP, Stick SM, Investigators AC. Risk factors for bronchiectasis in children with cystic fibrosis. *The New England journal of medicine* 2013; 368: 1963-1970.
10. Huber W, Carey VJ, Gentleman R, Anders S, Carlson M, Carvalho BS, Bravo HC, Davis S, Gatto L, Girke T, Gottardo R, Hahne F, Hansen KD, Irizarry RA, Lawrence M, Love MI, MacDonald J, Obenchain V, Oleś AK, Pagès H, Reyes A, Shannon P, Smyth GK, Tenenbaum D, Waldron L, Morgan M. Orchestrating high-throughput genomic analysis with Bioconductor. *Nature methods* 2015; 12: 115-121.

11. Lun ATL, Riesenfeld S, Andrews T, Dao TP, Gomes T, participants in the 1st Human Cell Atlas J, Marioni JC. EmptyDrops: distinguishing cells from empty droplets in droplet-based single-cell RNA sequencing data. *Genome biology* 2019; 20: 63-63.
12. Huang X, Huang Y. Cellsnp-lite: an efficient tool for genotyping single cells. *Bioinformatics* 2021.
13. Huang Y, McCarthy DJ, Stegle O. Vireo: Bayesian demultiplexing of pooled single-cell RNA-seq data without genotype reference. *Genome Biol* 2019; 20: 273.
14. Muskovic W, Powell JE. DropletQC: improved identification of empty droplets and damaged cells in single-cell RNA-seq data. *Genome Biology* 2021; 22: 329.
15. Hafemeister C, Satija R. Normalization and variance stabilization of single-cell RNA-seq data using regularized negative binomial regression. *Genome Biology* 2019; 20: 296.
16. Hao Y, Hao S, Andersen-Nissen E, Mauck WM, 3rd, Zheng S, Butler A, Lee MJ, Wilk AJ, Darby C, Zager M, Hoffman P, Stoeckius M, Papalexi E, Mimitou EP, Jain J, Srivastava A, Stuart T, Fleming LM, Yeung B, Rogers AJ, McElrath JM, Blish CA, Gottardo R, Smibert P, Satija R. Integrated analysis of multimodal single-cell data. *Cell* 2021; 184: 3573-3587.e3529.
17. Butler A, Hoffman P, Smibert P, Papalexi E, Satija R. Integrating single-cell transcriptomic data across different conditions, technologies, and species. *Nat Biotechnol* 2018; 36: 411-420.
18. Stuart T, Butler A, Hoffman P, Hafemeister C, Papalexi E, Mauck WM, 3rd, Hao Y, Stoeckius M, Smibert P, Satija R. Comprehensive Integration of Single-Cell Data. *Cell* 2019; 177: 1888-1902.e1821.
19. Stuart T, Satija R. Integrative single-cell analysis. *Nat Rev Genet* 2019; 20: 257-272.
20. Zappia L, Oshlack A. Clustering trees: a visualization for evaluating clusterings at multiple resolutions. *GigaScience* 2018; 7.
21. Sim CB, Phipson B, Ziemann M, Rafehi H, Mills RJ, Watt KI, Abu-Bonsrah KD, Kalathur RKR, Voges HK, Dinh DT, Ter Huurne M, Vivien CJ, Kaspi A, Kaipananickal H, Hidalgo A, Delbridge LMD, Robker RL, Gregorevic P, Dos Remedios CG, Lal S, Piers AT, Konstantinov IE, Elliott DA, El-Osta A, Oshlack A, Hudson JE, Porrello ER. Sex-Specific Control of Human Heart Maturation by the Progesterone Receptor. *Circulation* 2021.
22. Wu D, Smyth GK. Camera: a competitive gene set test accounting for inter-gene correlation. *Nucleic acids research* 2012; 40: e133-e133.
23. Mulè MP, Martins AJ, Tsang JS. Normalizing and denoising protein expression data from droplet-based single cell profiling. *Nat Commun* 2022; 13: 2099.
24. Kim HJ, Wang K, Chen C, Lin Y, Tam PPL, Lin DM, Yang JYH, Yang P. Uncovering cell identity through differential stability with Cepo. *Nature Computational Science* 2021; 1: 784-790.
25. Phipson B, Sim CB, Porrello E, Hewitt A, Powell J, Oshlack A. propeller : testing for differences in cell type proportions in single cell data. bioRxiv; 2021.
26. Benjamini Y, Hochberg Y. Controlling the False Discovery Rate - a Practical and Powerful Approach to Multiple Testing. *J R Stat Soc B* 1995; 57: 289-300.
27. Crowell HL, Soneson C, Germain P-L, Calini D, Collin L, Raposo C, Malhotra D, Robinson MD. muscat detects subpopulation-specific state transitions from multi-sample multi-condition single-cell transcriptomics data. *Nat Commun* 2020; 11: 6077.
28. Robinson MD, McCarthy DJ, Smyth GK. edgeR: a Bioconductor package for differential expression analysis of digital gene expression data. *Bioinformatics* 2009; 26: 139-140.
29. Chen Y, Lun AT, Smyth GK. From reads to genes to pathways: differential expression analysis of RNA-Seq experiments using Rsubread and the edgeR quasi-likelihood pipeline. *F1000Research* 2016; 5: 1438.

30. Ritchie ME, Phipson B, Wu D, Hu Y, Law CW, Shi W, Smyth GK. limma powers differential expression analyses for RNA-sequencing and microarray studies. *Nucleic acids research* 2015; 43: e47.
31. Law CW, Chen Y, Shi W, Smyth GK. voom: precision weights unlock linear model analysis tools for RNA-seq read counts. *Genome Biology* 2014; 15: R29.
32. Phipson B, Lee S, Majewski IJ, Alexander WS, Smyth GK. Robust hyperparameter estimation protects against hypervariable genes and improves power to detect differential expression. *The Annals of Applied Statistics* 2016; 10: 946-963, 918.
33. McCarthy DJ, Smyth GK. Testing significance relative to a fold-change threshold is a TREAT. *Bioinformatics* 2009; 25: 765-771.
34. Phipson B, Maksimovic J, Oshlack A. missMethyl: an R package for analyzing data from Illumina's HumanMethylation450 platform. *Bioinformatics* 2016; 32: 286-288.
35. Blischak JD, Carbonetto P, Stephens M. Creating and sharing reproducible research code the workflowr way. *F1000Research* 2019; 8: 1749.
36. Liao Z, Jin Y, Chu Y, Wu H, Li X, Deng Z, Feng S, Chen N, Luo Z, Zheng X, Bao L, Xu Y, Tan H, Zhao L. Single-cell transcriptome analysis reveals aberrant stromal cells and heterogeneous endothelial cells in alcohol-induced osteonecrosis of the femoral head. *Commun Biol* 2022; 5: 324.
37. Crinier A, Dumas P-Y, Escalière B, Piperoglou C, Gil L, Villacreces A, Vély F, Ivanovic Z, Milpied P, Narni-Mancinelli É, Vivier É. Single-cell profiling reveals the trajectories of natural killer cell differentiation in bone marrow and a stress signature induced by acute myeloid leukemia. *Cellular & molecular immunology* 2021; 18: 1290-1304.
38. Mattiola I, Tomay F, De Pizzol M, Silva-Gomes R, Savino B, Gulic T, Doni A, Lonardi S, Astrid Boutet M, Nerviani A, Carriero R, Molgora M, Stravalaci M, Morone D, Shalova IN, Lee Y, Biswas SK, Mantovani G, Sironi M, Pitzalis C, Vermi W, Bottazzi B, Mantovani A, Locati M. The macrophage tetraspan MS4A4A enhances dectin-1-dependent NK cell-mediated resistance to metastasis. *Nat Immunol* 2019; 20: 1012-1022.
39. Bissonnette EY, Lauzon-Joset J-F, Debley JS, Ziegler SF. Cross-Talk Between Alveolar Macrophages and Lung Epithelial Cells is Essential to Maintain Lung Homeostasis. *Frontiers in immunology* 2020; 11.
40. Morrell ED, Wiedeman A, Long SA, Gharib SA, West TE, Skerrett SJ, Wurfel MM, Mikacenic C. Cytometry TOF identifies alveolar macrophage subtypes in acute respiratory distress syndrome. *JCI Insight* 2018; 3.
41. Kraft S, Jouvin M-H, Kulkarni N, Kissing S, Morgan ES, Dvorak AM, Schröder B, Saftig P, Kinet J-P. The tetraspanin CD63 is required for efficient IgE-mediated mast cell degranulation and anaphylaxis. *Journal of immunology (Baltimore, Md : 1950)* 2013; 191: 2871-2878.
42. Grieshaber-Bouyer R, Radtke FA, Cunin P, Stifano G, Levescot A, Vijaykumar B, Nelson-Maney N, Blaustein RB, Monach PA, Nigrovic PA, Aguilar O, Allan R, Astarita J, Austen KF, Barrett N, Baysoy A, Benoist C, Brown BD, Buechler M, Buenrostro J, Casanova MA, Chowdhary K, Colonna M, Crowl T, Deng T, Desland F, Dhainaut M, Ding J, Dominguez C, Dwyer D, Frascoli M, Gal-Oz S, Goldrath A, Johanson T, Jordan S, Kang J, Kapoor V, Kenigsberg E, Kim J, Kim Kw, Kiner E, Kronenberg M, Lanier L, Laplace C, Lareau C, Leader A, Lee J, Magen A, Maier B, Maslova A, Mathis D, McFarland A, Merad M, Meunier E, Monach PA, Mostafavi S, Muller S, Muus C, Ner-Gaon H, Nguyen Q, Novakovsky G, Nutt S, Omilusik K, Ortiz-Lopez A, Paynich M, Peng V, Potempa M, Pradhan R, Quon S, Ramirez R, Ramanan D, Randolph G, Regev A, Rose SA, Seddu K, Shay T, Shemesh A, Shyer J,

Smilie C, Spidale N, Subramanian A, Sylvia K, Tellier J, Turley S, Vijaykumar B, Wagers A, Wang C, Wang PL, Wroblewska A, Yang L, Yim A, Yoshida H, ImmGen C. The neutrotime transcriptional signature defines a single continuum of neutrophils across biological compartments. *Nat Commun* 2021; 12: 2856.

43. Shanthikumar S, Ranganathan SC, Saffery R, Neeland MR. Mapping Pulmonary and Systemic Inflammation in Preschool Aged Children With Cystic Fibrosis. *Frontiers in immunology* 2021; 12: 733217.
44. Zilionis R, Engblom C, Pfirschke C, Savova V, Zemmour D, Saatcioglu HD, Krishnan I, Maroni G, Meyerovitz CV, Kerwin CM, Choi S, Richards WG, De Rienzo A, Tenen DG, Bueno R, Levantini E, Pittet MJ, Klein AM. Single-Cell Transcriptomics of Human and Mouse Lung Cancers Reveals Conserved Myeloid Populations across Individuals and Species. *Immunity* 2019; 50: 1317-1334.e1310.
45. Vandendriessche S, Cambier S, Proost P, Marques PE. Complement Receptors and Their Role in Leukocyte Recruitment and Phagocytosis. *Frontiers in Cell and Developmental Biology* 2021; 9.
46. Abdel-Salam BK, Ebaid H. Expression of CD11b and CD18 on polymorphonuclear neutrophils stimulated with interleukin-2. *Cent Eur J Immunol* 2014; 39: 209-215.
47. Haziot A, Tsuberi BZ, Goyert SM. Neutrophil CD14: biochemical properties and role in the secretion of tumor necrosis factor-alpha in response to lipopolysaccharide. *J Immunol* 1993; 150: 5556-5565.
48. Silva-Gomes R, Mapelli SN, Boutet MA, Mattiola I, Sironi M, Grizzi F, Colombo F, Supino D, Carnevale S, Pasqualini F, Stravalaci M, Porte R, Gianatti A, Pitzalis C, Locati M, Oliveira MJ, Bottazzi B, Mantovani A. Differential expression and regulation of MS4A family members in myeloid cells in physiological and pathological conditions. *J Leukoc Biol* 2022; 111: 817-836.
49. Munthe-Fog L, Hummelshoj T, Honoré C, Moller ME, Skjoedt MO, Palsgaard I, Borregaard N, Madsen HO, Garred P. Variation in FCN1 affects biosynthesis of ficolin-1 and is associated with outcome of systemic inflammation. *Genes & Immunity* 2012; 13: 515-522.
50. Tan SYS, Krasnow MA. Developmental origin of lung macrophage diversity. *Development* 2016; 143: 1318-1327.
51. Gillespie M, Jassal B, Stephan R, Milacic M, Rothfels K, Senff-Ribeiro A, Griss J, Sevilla C, Matthews L, Gong C, Deng C, Varusai T, Ragueneau E, Haider Y, May B, Shamovsky V, Weiser J, Brunson T, Sanati N, Beckman L, Shao X, Fabregat A, Sidiropoulos K, Murillo J, Viteri G, Cook J, Shorser S, Bader G, Demir E, Sander C, Haw R, Wu G, Stein L, Hermjakob H, D'Eustachio P. The reactome pathway knowledgebase 2022. *Nucleic acids research* 2021; 50: D687-D692.
52. Figenschau SL, Knutsen E, Urbarova I, Fenton C, Elston B, Perander M, Mortensen ES, Fenton KA. ICAM1 expression is induced by proinflammatory cytokines and associated with TLS formation in aggressive breast cancer subtypes. *Scientific reports* 2018; 8: 11720.
53. Oakley MS, Chorazeczewski JK, Aleshnick M, Anantharaman V, Majam V, Chawla B, Myers TG, Su Q, Okoth WA, Takeda K, Akue A, KuKuruga M, Aravind L, Kumar S. TCRβ-expressing macrophages induced by a pathogenic murine malaria correlate with parasite burden and enhanced phagocytic activity. *PLoS One* 2018; 13: e0201043.
54. Rodriguez-Cruz A, Vesin D, Ramon-Luing L, Zuñiga J, Quesniaux VFJ, Ryffel B, Lascurain R, Garcia I, Chávez-Galán L. CD3+ Macrophages Deliver Proinflammatory Cytokines by a CD3- and Transmembrane TNF-Dependent Pathway and Are Increased at the BCG-Infection Site. *Frontiers in immunology* 2019; 10.

55. Loske J, Röhmel J, Lukassen S, Stricker S, Magalhães VG, Liebig J, Chua RL, Thürmann L, Messingschlager M, Seegebarth A, Timmermann B, Klages S, Ralser M, Sawitzki B, Sander LE, Corman VM, Conrad C, Laudi S, Binder M, Trump S, Eils R, Mall MA, Lehmann I. Pre-activated antiviral innate immunity in the upper airways controls early SARS-CoV-2 infection in children. *Nat Biotechnol* 2022; 40: 319-324.
56. Zheng MZM, Wakim LM. Tissue resident memory T cells in the respiratory tract. *Mucosal Immunol* 2021.
57. Bengsch B, Ohtani T, Herati RS, Bovenschen N, Chang K-M, Wherry EJ. Deep immune profiling by mass cytometry links human T and NK cell differentiation and cytotoxic molecule expression patterns. *J Immunol Methods* 2018; 453: 3-10.
58. Weinstein JS, Lezon-Geyda K, Maksimova Y, Craft S, Zhang Y, Su M, Schulz VP, Craft J, Gallagher PG. Global transcriptome analysis and enhancer landscape of human primary T follicular helper and T effector lymphocytes. *Blood* 2014; 124: 3719-3729.
59. Minoda Y, Virshup I, Leal Rojas I, Haigh O, Wong Y, Miles JJ, Wells CA, Radford KJ. Human CD141+ Dendritic Cell and CD1c+ Dendritic Cell Undergo Concordant Early Genetic Programming after Activation in Humanized Mice In Vivo. *Frontiers in immunology* 2017; 8.
60. Tullett KM, Lahoud MH, Radford KJ. Harnessing Human Cross-Presenting CLEC9A+XCR1+ Dendritic Cells for Immunotherapy. *Frontiers in immunology* 2014; 5.
61. Collin M, McGovern N, Haniffa M. Human dendritic cell subsets. *Immunology* 2013; 140: 22-30.
62. da Silva FAR, Pascoal LB, Dotti I, Setsuko Ayrizono MdL, Aguilar D, Rodrigues BL, Arroyes M, Ferrer-Picon E, Milanski M, Velloso LA, Fagundes JJ, Salas A, Leal RF. Whole transcriptional analysis identifies markers of B, T and plasma cell signaling pathways in the mesenteric adipose tissue associated with Crohn's disease. *J Transl Med* 2020; 18: 44.
63. Baßler K, Fujii W, Kapellos TS, Horne A, Reiz B, Dudkin E, Lücken M, Reusch N, Osei-Sarpong C, Warnat-Herresthal S, Wagner A, Bonaguro L, Günther P, Pizarro C, Schreiber T, Becker M, Händler K, Wohnhaas CT, Baumgartner F, Köhler M, Theis H, Kraut M, Wadsworth MH, Hughes TK, Ferreira HJG, Schulte-Schrepping J, Hinkley E, Kaltheuner IH, Geyer M, Thiele C, Shalek AK, Feißt A, Thomas D, Dickten H, Beyer M, Baum P, Yosef N, Aschenbrenner AC, Ulas T, Hasenauer J, Theis FJ, Skowasch D, Schultze JL. Alterations of multiple alveolar macrophage states in chronic obstructive pulmonary disease. *bioRxiv* 2020: 2020.2005.2028.121541.
64. Bruscia EM, Bonfield TL. Cystic Fibrosis Lung Immunity: The Role of the Macrophage. *J Innate Immun* 2016; 8: 550-563.
65. Giacalone VD, Dobosh BS, Gaggar A, Tirouvanziam R, Margaroli C. Immunomodulation in Cystic Fibrosis: Why and How? *International Journal of Molecular Sciences* 2020; 21: 3331.
66. Savin IA, Markov AV, Zenkova MA, Sen'kova AV. Asthma and Post-Asthmatic Fibrosis: A Search for New Promising Molecular Markers of Transition from Acute Inflammation to Pulmonary Fibrosis. *Biomedicines* 2022; 10: 1017.
67. Michalec L, Choudhury BK, Postlethwait E, Wild JS, Alam R, Lett-Brown M, Sur S. CCL7 and CXCL10 orchestrate oxidative stress-induced neutrophilic lung inflammation. *J Immunol* 2002; 168: 846-852.
68. Gabryelska A, Kuna P, Antczak A, Białasiewicz P, Panek M. IL-33 Mediated Inflammation in Chronic Respiratory Diseases-Understanding the Role of the Member of IL-1 Superfamily. *Frontiers in immunology* 2019; 10: 692.

69. Tiringer K, Treis A, Kanolzer S, Witt C, Ghanim B, Gruber S, Schmidthaler K, Renner S, Dehlink E, Nachbaur E, Frischer T, Klepetko W, Akdis CA, Szépfalusi Z, Eiwegger T. Differential expression of IL-33 and HMGB1 in the lungs of stable cystic fibrosis patients. *European Respiratory Journal* 2014; 44: 802-805.
70. Tyler A, Mahoney JM, Carter GW. Genetic Interactions Affect Lung Function in Patients with Systemic Sclerosis. *G3 Genes|Genomes|Genetics* 2020; 10: 151-163.
71. Robbesom AA, Koenders MM, Smits NC, Hafmans T, Versteeg EM, Bulten J, Veerkamp JH, Dekhuijzen PN, van Kuppevelt TH. Aberrant fibrillin-1 expression in early emphysematous human lung: a proposed predisposition for emphysema. *Mod Pathol* 2008; 21: 297-307.
72. Morse C, Tabib T, Sembrat J, Buschur KL, Bittar HT, Valenzi E, Jiang Y, Kass DJ, Gibson K, Chen W, Mora A, Benos PV, Rojas M, Lafyatis R. Proliferating SPP1/MERTK-expressing macrophages in idiopathic pulmonary fibrosis. *The European respiratory journal* 2019; 54.
73. Wang T, Jin H, Hu J, Li X, Ruan H, Xu H, Wei L, Dong W, Teng F, Gu J, Qin W, Luo X, Hao Y. COL4A1 promotes the growth and metastasis of hepatocellular carcinoma cells by activating FAK-Src signaling. *Journal of Experimental & Clinical Cancer Research* 2020; 39: 148.
74. Gaudet P, Livstone MS, Lewis SE, Thomas PD. Phylogenetic-based propagation of functional annotations within the Gene Ontology consortium. *Brief Bioinform* 2011; 12: 449-462.
75. Schupp JC, Khanal S, Gomez JL, Sauler M, Adams TS, Chupp GL, Yan X, Poli S, Zhao Y, Montgomery RR, Rosas IO, Dela Cruz CS, Bruscia EM, Egan ME, Kaminski N, Britto CJ. Single-Cell Transcriptional Archetypes of Airway Inflammation in Cystic Fibrosis. *American journal of respiratory and critical care medicine* 2020; 202: 1419-1429.
76. Bian Z, Gong Y, Huang T, Lee CZW, Bian L, Bai Z, Shi H, Zeng Y, Liu C, He J, Zhou J, Li X, Li Z, Ni Y, Ma C, Cui L, Zhang R, Chan JKY, Ng LG, Lan Y, Ginhoux F, Liu B. Deciphering human macrophage development at single-cell resolution. *Nature* 2020; 582: 571-576.

FIGURE LEGENDS

Figure 1. Broad immune and epithelial cell profile of the paediatric lung. **(A)** Multimodal experimental design: 12 cryopreserved bronchoalveolar (BAL) samples from children aged 3-6 years were thawed and sorted by FACS for live, single cells. These cells underwent scRNA-seq, CITE-seq, or flow cytometry as specified and were analysed to create a cell atlas of the paediatric lower airway. **(B)** UMAP visualisation of broad immune and epithelial cell populations, coloured by cell type. **(C)** Proportions of each broad population in each participant **(D)** Most significant marker genes for each broad population. **(E)** Expression of TotalSeq antibody derived tags (ADT) for immune cell lineage markers in each broad cell population for 8 samples that were analysed by CITE-seq. Endothelial cells were only identified in 2 participants whose samples were analysed by scRNA-seq, so there is no ADT data for this cell type.

Figure 2. Flow cytometry analysis of BAL samples and comparison with scRNA-seq. **(A)** UMAP depicting major cell populations identified by spectral flow cytometry of 7 samples: B cells, CD4 T cells, CD8 T cells, dendritic cells, macrophages, monocytes, neutrophils and airway epithelial cells. **(B)** Cell proportions identified by scRNA-seq and flow cytometry in samples from individuals that received both techniques (participants F2-L2). Common cell types identified in both datasets are shown. All cell types identified by scRNA-seq are shown in Figure 1. **(C)** Statistical comparison of the difference in proportions identified by flow cytometry and scRNA-seq. *indicates cell types where a significant difference was observed. **(D)** Cell type specific protein expression by flow cytometry for markers included in the panel: CD15, CD66b, CD16, CD11c, CD14, CD45, CD19, CD47, HLA-DR, CD63, CD172α, CD206, CD4, CD4, CD8, CD279 (PD1), and EPCAM.

Figure 3. Identification of functionally distinct alveolar macrophage subpopulations. **(A)** UMAP visualisation of macrophage subpopulations identified by a subclustering analysis of cells within the total macrophage pool. **(B)** Proportions (as a percent of all macrophages) of each macrophage subpopulation in each participant. **(C)** Most significant marker genes for each macrophage subpopulation. **(D)** Expression of relevant TotalSeq antibody derived tags (ADT) in each macrophage subpopulation for 8 samples that were analysed by CITE-seq.

Figure 4. Characterisation of distinct T and NK cell subsets. **(A)** UMAP visualisation of T and NK cell subsets identified by a subclustering analysis of cells within the 'T/NK' group. **(B)** Most significant marker genes for each identified T and NK cell subset. **(C)** Expression of TotalSeq antibody derived tags (ADT) for T and NK cell markers in each cell subset for 8 samples that were analysed by CITE-seq. CD4 TFH cells were only identified in 1 participant whose sample was analysed by scRNA-seq, so there is no ADT data for this cell type.

Figure 5. Characterisation of rare myeloid, B cell and epithelial cell population. **(A)** UMAP visualisation of cell subsets identified by a subclustering analysis of cells within the 'not macrophage, not T/NK' population. **(B)** Most significant marker genes for each cell subset. **(C)** Expression of relevant TotalSeq antibody derived tags (ADT) in each cell subset for 8 samples that were analysed by CITE-seq. Endothelial cells were only identified in 2 participants whose samples were analysed by scRNA-seq, so there is no ADT data for this cell type.

Figure 6. Altered macrophage gene expression in cystic fibrosis. **(A)** Volcano plot depicting differentially expressed genes in the broad macrophage population between healthy and CF samples. Red: upregulated in control compared to CF, blue: downregulated in control compared to CF, grey: not significantly different between the two groups. **(B)** Heatmap depicting individual expression levels of all 58 differentially expressed genes in the broad macrophage population between healthy and CF samples. Variables including disease [CF or control], sex [female (F) or male (M)], age [3-6 years], and batch [1 (scRNA-seq) or 2 (CITE-seq)] are shown.

ACKNOWLEDGEMENTS

The authors would like to acknowledge the generous support and guidance provided by Professor Daniel Chambers and Dr Brendan O'Sullivan regarding experimental methods when designing the first study. We thank the children and parents who participated in the AREST-CF study, without whom this work would not have been possible.

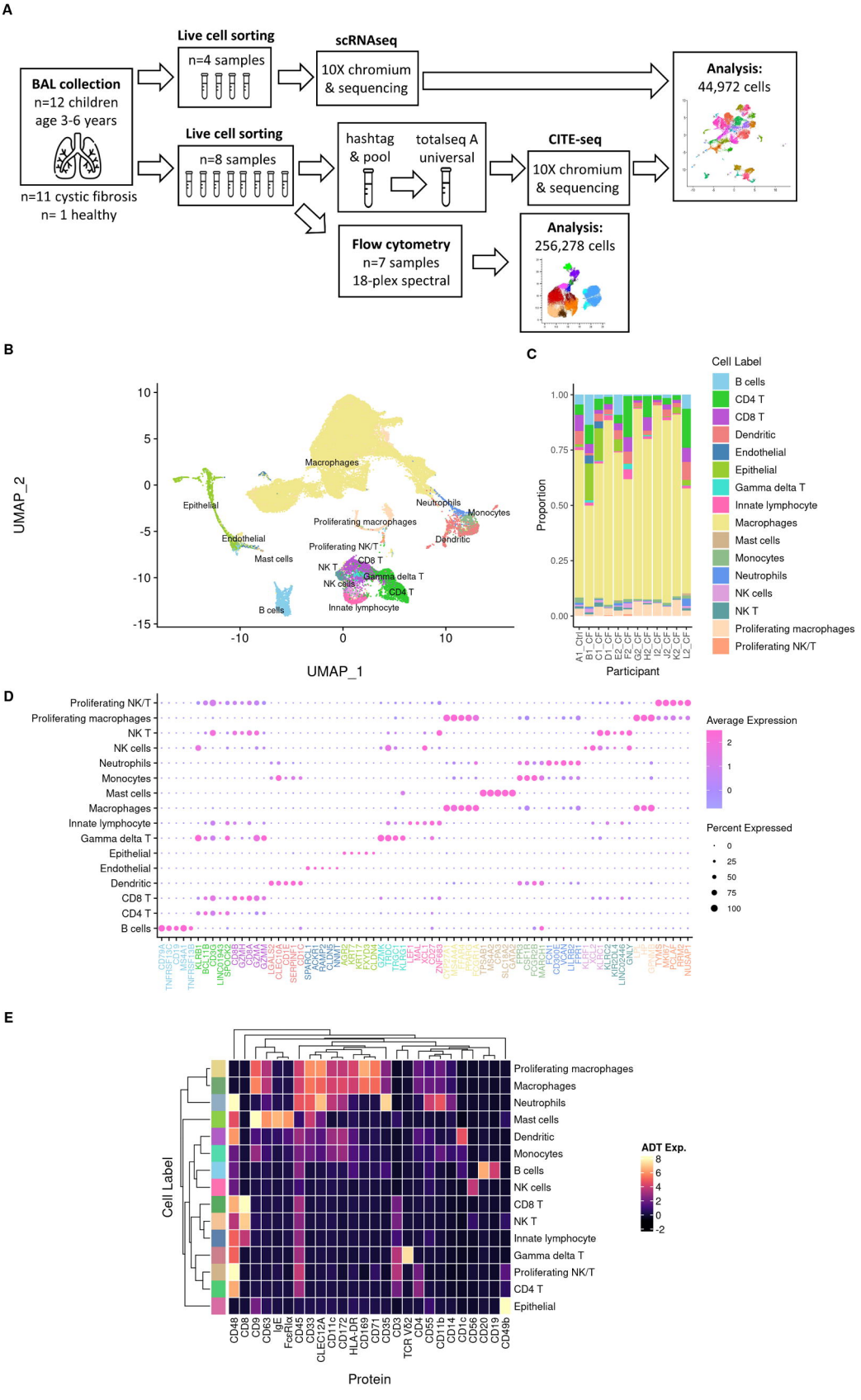
A
BAL collection
n=12 children
age 3-6 years
n=11 cystic fibrosis
n= 1 healthy
Live cell sorting
n=4 samples
scRNAseq
10X chromium
& sequencing
Analysis:
44,972 cells
Live cell sorting
n=8 samples
hashtag
& pool
totalseq A
universal
CITE-seq
10X chromium
& sequencing
Flow cytometry
n=7 samples
18-plex spectral
Analysis:
256,278 cells
B
UMAP_2
UMAP_1
Macrophages
Epithelial
Neutrophils
Monocytes
Proliferating macrophages
Endothelial
Proliferating NK/T
Dendritic
Mast cells
CD8 T
NK T
Gamma delta T
NK cells
CD4 T
B cells
Innate lymphocyte
C
Proportion
Participant
Cell Label
B cells
CD4 T
CD8 T
Dendritic
Endothelial
Epithelial
Gamma delta T
Innate lymphocyte
Macrophages
Mast cells
Monocytes
Neutrophils
NK cells
NK T
Proliferating macrophages
Proliferating NK/T
D
Average Expression
Percent Expressed
E
Cell Label
Protein
ADT Exp.

Figure 1

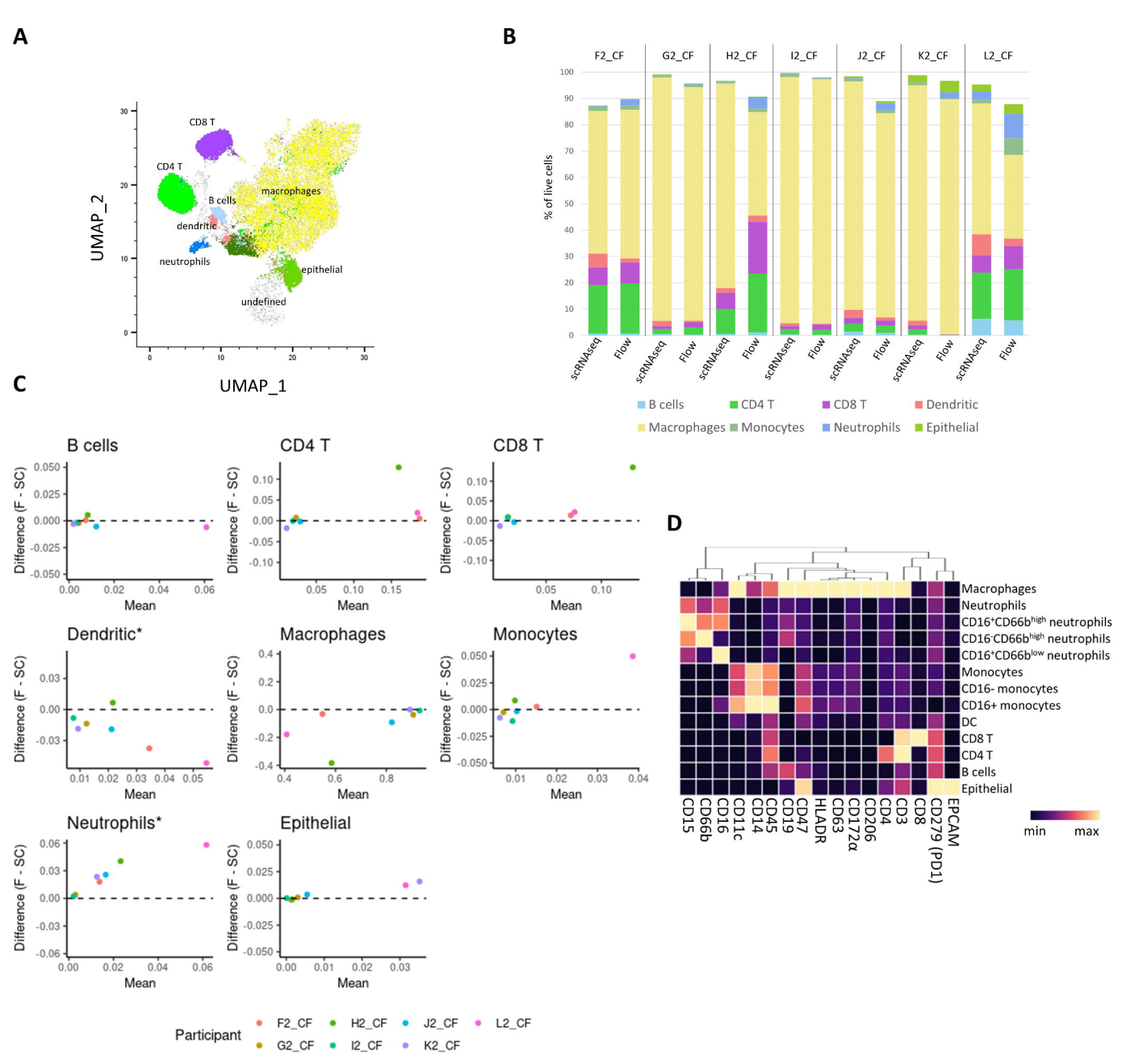
A
CD8 T
CD4 T
B cells
macrophages
dendritic
neutrophils
epithelial
undefined
UMAP_2
UMAP_1
B
F2_CF
G2_CF
H2_CF
I2_CF
J2_CF
K2_CF
L2_CF
% of live cells
scRNAseq
Flow
B cells
CD4 T
CD8 T
Dendritic
Macrophages
Monocytes
Neutrophils
Epithelial
C
B cells
CD4 T
CD8 T
Dendritic*
Macrophages
Monocytes
Neutrophils*
Epithelial
Difference (F - SC)
Mean
Participant
F2_CF
G2_CF
H2_CF
I2_CF
J2_CF
K2_CF
L2_CF
D
Macrophages
Neutrophils
CD16+CD66bhigh neutrophils
CD16-CD66bhigh neutrophils
CD16+CD66blow neutrophils
Monocytes
CD16- monocytes
CD16+ monocytes
DC
CD8 T
CD4 T
B cells
Epithelial
CD15
CD66b
CD16
CD11c
CD14
CD45
CD19
CD47
HLADR
CD63
CD172α
CD206
CD4
CD3
CD8
CD279 (PD1)
EPCAM
min
max

Figure 2

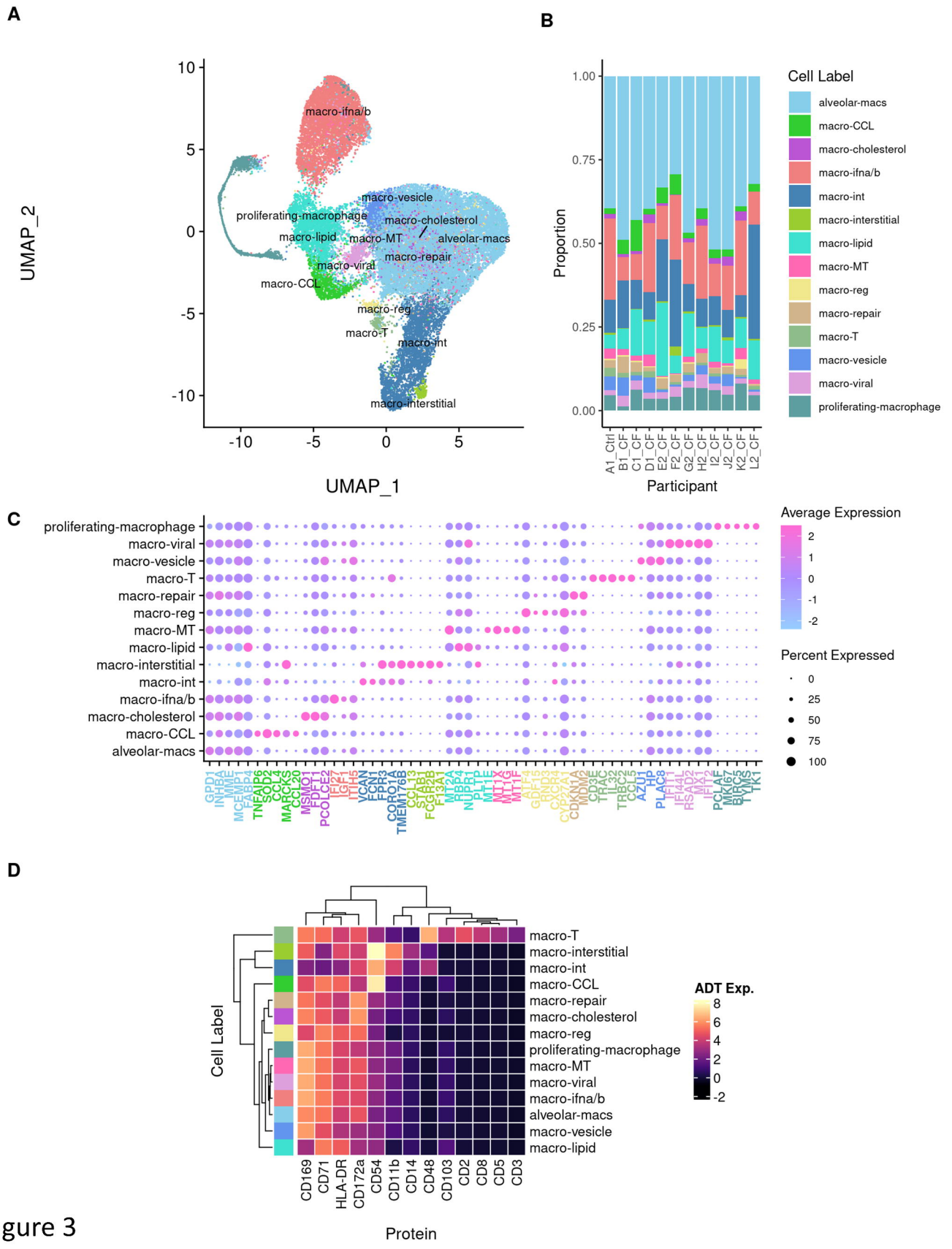
A
UMAP_2
UMAP_1
macro-ifna/b
macro-vesicle
proliferating-macrophage
macro-cholesterol
macro-lipid
macro-MT
alveolar-macs
macro-repair
macro-viral
macro-CCL
macro-reg
macro-T
macro-int
macro-interstitial
B
Proportion
Participant
A1_Ctrl
B1_CF
C1_CF
D1_CF
E2_CF
F2_CF
G2_CF
H2_CF
I2_CF
J2_CF
K2_CF
L2_CF
Cell Label
alveolar-macs
macro-CCL
macro-cholesterol
macro-ifna/b
macro-int
macro-interstitial
macro-lipid
macro-MT
macro-reg
macro-repair
macro-T
macro-vesicle
macro-viral
proliferating-macrophage
C
Average Expression
Percent Expressed
D
Cell Label
Protein
ADT Exp.
CD169
CD71
HLA-DR
CD172a
CD54
CD11b
CD14
CD48
CD103
CD2
CD8
CD5
CD3

Figure 3

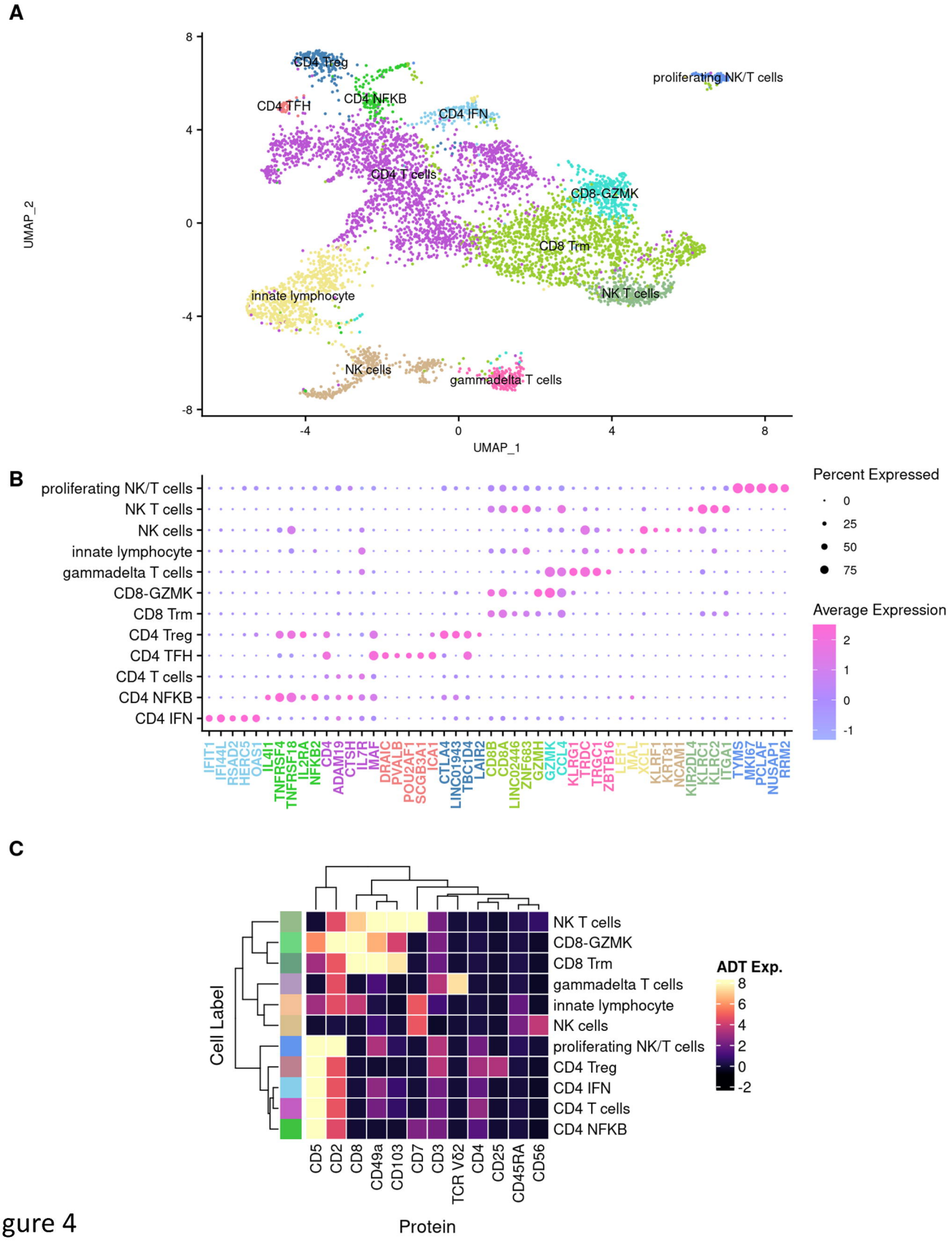
A
CD4 Treg
CD4 TFH
CD4 NFKB
CD4 IFN
proliferating NK/T cells
CD4 T cells
CD8-GZMK
CD8 Trm
innate lymphocyte
NK T cells
NK cells
gammadelta T cells
UMAP_2
UMAP_1
B
proliferating NK/T cells
NK T cells
NK cells
innate lymphocyte
gammadelta T cells
CD8-GZMK
CD8 Trm
CD4 Treg
CD4 TFH
CD4 T cells
CD4 NFKB
CD4 IFN
Percent Expressed
Average Expression
C
Cell Label
ADT Exp.
Protein
CD5
CD2
CD8
CD49a
CD103
CD7
CD3
TCR V62
CD4
CD25
CD45RA
CD56

Figure 4

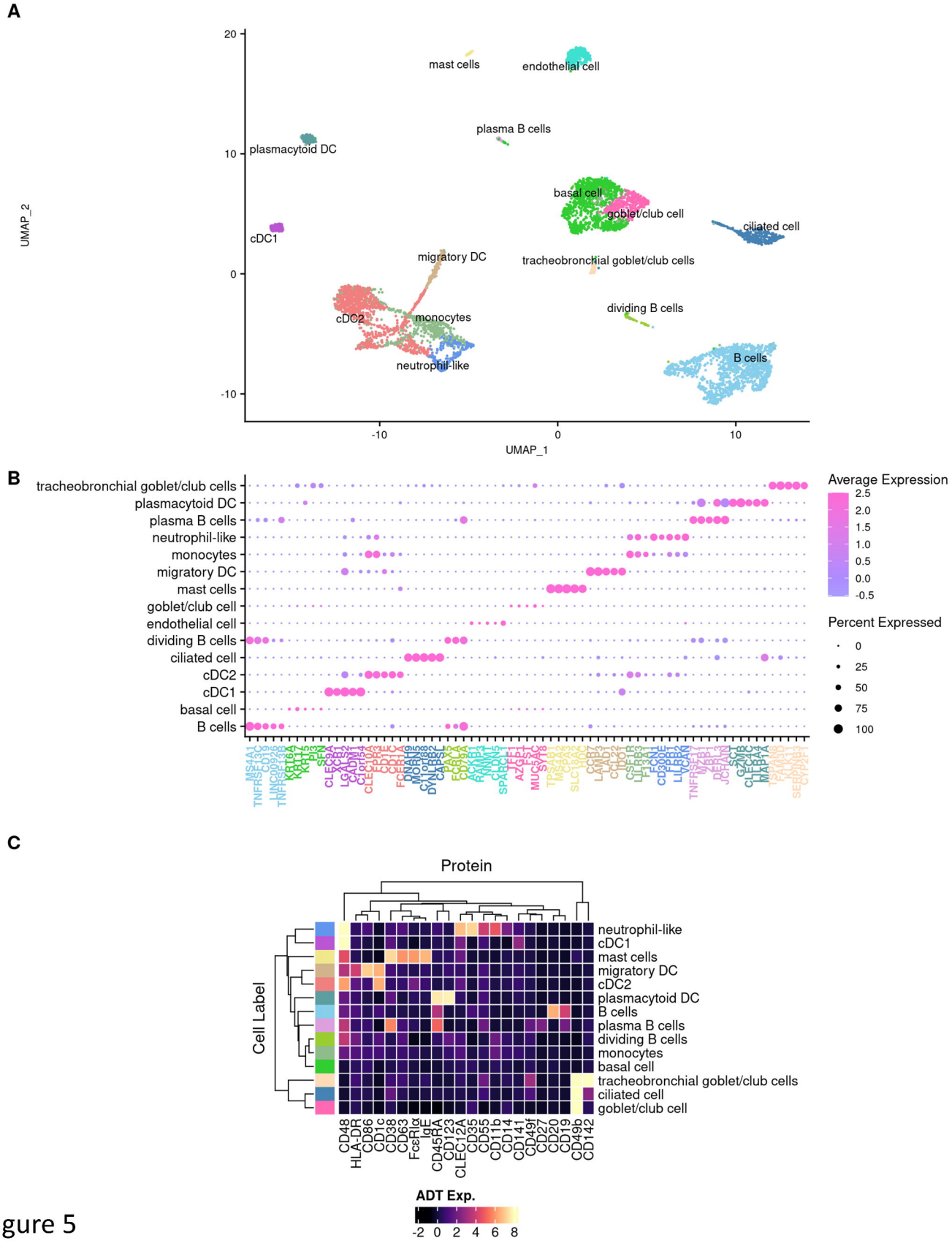
A
mast cells
endothelial cell
plasma B cells
plasmacytoid DC
basal cell
goblet/club cell
ciliated cell
cDC1
migratory DC
tracheobronchial goblet/club cells
dividing B cells
cDC2
monocytes
neutrophil-like
B cells
UMAP_2
UMAP_1
B
tracheobronchial goblet/club cells
plasmacytoid DC
plasma B cells
neutrophil-like
monocytes
migratory DC
mast cells
goblet/club cell
endothelial cell
dividing B cells
ciliated cell
cDC2
cDC1
basal cell
B cells
Average Expression
Percent Expressed
C
Protein
Cell Label
neutrophil-like
cDC1
mast cells
migratory DC
cDC2
plasmacytoid DC
B cells
plasma B cells
dividing B cells
monocytes
basal cell
tracheobronchial goblet/club cells
ciliated cell
goblet/club cell
CD48
HLA-DR
CD86
CD1c
CD38
CD63
FcεRIα
IgE
CD45RA
CD123
CLEC12A
CD35
CD55
CD11b
CD14
CD141
CD49f
CD27
CD20
CD19
CD49b
CD142
ADT Exp.

Figure 5

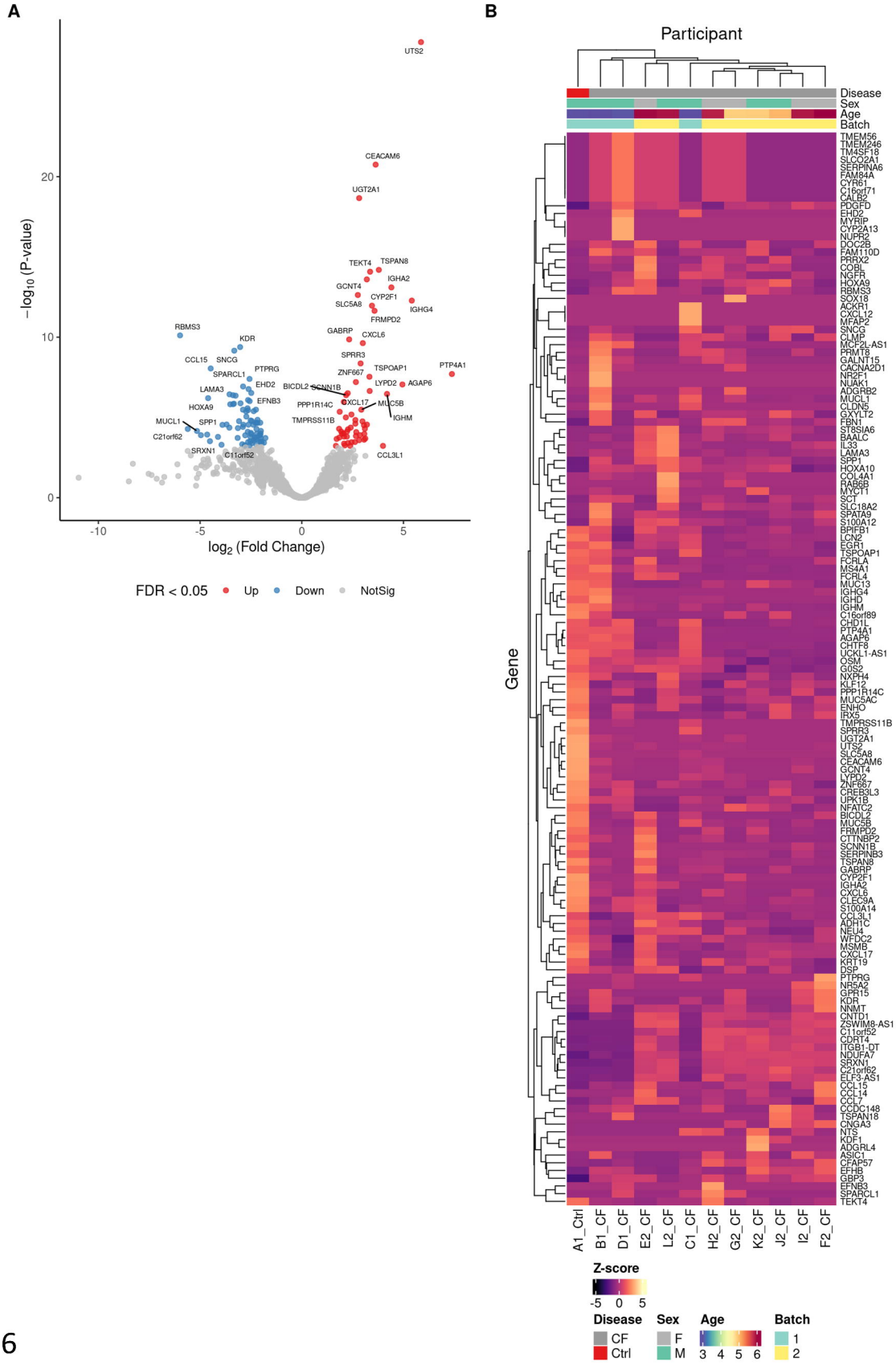
A
B
Participant
Disease
Sex
Age
Batch
Gene
Z-score
-5 0 5
Disease
CF
Ctrl
Sex
F
M
Age
3 4 5 6
Batch
1
2
A1_Ctrl
B1_CF
D1_CF
E2_CF
L2_CF
C1_CF
H2_CF
G2_CF
K2_CF
J2_CF
I2_CF
F2_CF
−log10 (P-value)
log2 (Fold Change)
FDR < 0.05
Up
Down
NotSig
UTS2
CEACAM6
UGT2A1
TEKT4
TSPAN8
IGHA2
GCNT4
CYP2F1
SLC5A8
IGHG4
FRMPD2
GABRP
CXCL6
SPRR3
ZNF667
TSPOAP1
PTP4A1
LYPD2
AGAP6
BICDL2
SCNN1B
CXCL17
MUC5B
IGHM
PPP1R14C
TMPRSS11B
CCL3L1
RBMS3
KDR
CCL15
SNCG
PTPRG
SPARCL1
EHD2
LAMA3
EFNB3
HOXA9
MUCL1
SPP1
C21orf62
SRXN1
C11orf52

Figure 6